

MIT Open Access Articles

Terrestrial Evaporation and Moisture Drainage in a Warmer Climate

The MIT Faculty has made this article openly available. **Please share** how this access benefits you. Your story matters.

Citation: Short Gianotti, Daniel J., Akbar, Ruzbeh, Feldman, Andrew F., Salvucci, Guido D. and Entekhabi, Dara. 2020. "Terrestrial Evaporation and Moisture Drainage in a Warmer Climate." *Geophysical Research Letters*, 47 (5).

As Published: <http://dx.doi.org/10.1029/2019gl086498>

Publisher: American Geophysical Union (AGU)

Persistent URL: <https://hdl.handle.net/1721.1/140527>

Version: Author's final manuscript: final author's manuscript post peer review, without publisher's formatting or copy editing

Terms of use: Creative Commons Attribution-Noncommercial-Share Alike



Short Gianotti Daniel, J. (Orcid ID: 0000-0003-4891-2474)

Akbar Ruzbeh (Orcid ID: 0000-0002-9963-0488)

Feldman Andrew, F. (Orcid ID: 0000-0003-1547-6995)

Salvucci Guido, D. (Orcid ID: 0000-0003-3609-5972)

Terrestrial Evaporation and Moisture Drainage in a Warmer Climate

Daniel J. Short Gianotti¹, Ruzbeh Akbar¹, Andrew F. Feldman¹, Guido D. Salvucci², and
Dara Entekhabi¹

¹Parsons Laboratory, Department of Civil and Environmental Engineering, Massachusetts
Institute of Technology.

²Department of Earth and Environment, Boston University.

Corresponding author: Daniel Short Gianotti (gianotti@mit.edu)

Key Points:

- Aridity indices (Budyko) fail to capture effects of daily dynamics and precipitation extremes on long-term hydroclimate change
- Climate perturbations to evaporation/drainage are superposable despite nonlinear flux mechanisms and mixed-sign effects
- Long-term soil drying tied to trends in increased evaporation, decreased drainage to groundwater, streamflow

This is the author manuscript accepted for publication and has undergone full peer review but has not been through the copyediting, typesetting, pagination and proofreading process, which may lead to differences between this version and the Version of Record. Please cite this article as doi: [10.1029/2019GL086498](https://doi.org/10.1029/2019GL086498)

Abstract

To determine hydrologic changes in a warmer climate, we impose precipitation and potential evaporation (E_o) perturbations on hydrologic response functions constructed from precipitation and satellite soil moisture observations across the United States. Despite nonlinearities in the evaporation (E) and drainage (D) responses and opposing-sign perturbations, changes in individual fluxes are superposable. Empirical frameworks (Budyko) can misrepresent changes in E/D partitioning by neglecting shifts/trends in hydrologic regime and subseasonal precipitation dynamics. E/D both increase to balance mean precipitation (\bar{P}) increases, and increased E_o reduces soil moisture. E and D are generally more elastic to changes in \bar{P} than E_o . The results suggest that (1) the impacts of regional hydrologic perturbations may allow for simple superposition/scaling, (2) changes in timing/intensity of precipitation may have substantial impacts on mean moisture states and fluxes, and (3) changes to the distribution of surface moisture states are likely more relevant for E/D partitioning than common aridity indices.

Plain Language Summary

We use satellite observations of soil moisture and expected increase in air temperature to determine how evaporation and soil drainage (to groundwater recharge and rivers/streamflow) will change in a warmer climate. The impacts of drier air, more rainfall, and more extreme rainfall (drier dry days and wetter wet days) can largely be considered separately and then added, which will help when predicting a specific location's water balance using scenarios from global climate models. In typical scenarios, soils are likely to dry, evaporation is likely to increase, and — when precipitation increases — drainage to groundwater/streams is likely to increase as well. Evaporation and drainage are relatively more sensitive to changes in precipitation and humidity in the Western US than the East, and the Corn Belt is particularly susceptible to changes in precipitation intensity. Common methods of determining changes in evaporation and drainage which neglect changes in soil moisture may have large errors in global change scenarios.

Introduction

Our best predictions for the future of the terrestrial water cycle come from Global Climate and Earth System Models (GCMs, ESMs), which forecast general increases in precipitation (Greve et al., 2018; O’Gorman et al., 2012; O’Gorman & Schneider, 2008) and atmospheric water demand (Q. Fu & Feng, 2014), along with distributional changes in precipitation intensity (Greve et al., 2014; Hirabayashi et al., 2013; Schewe et al., 2014). The spatial patterns of these changes are driven by the coupling between radiative processes, cloud physics, and moisture advection, and are affected to a large degree by unpredictable internal variability in global atmospheric dynamics (Anderson et al., 2015; Greve et al., 2018; Greve & Seneviratne, 2015; Hawkins & Sutton, 2011; Samset et al., 2016). The modeled land-surface response to these changes is represented through parameterizations — as simple as single functions or as complex as a land-surface biosphere model — and is rarely separated from the uncertain atmospheric drivers or confronted with observations (Berg et al., 2017).

Water cycle changes are often summarized as changes in an aridity index — typically the ratio of mean precipitation (P) to mean potential evaporation (E_o) — following well-known hydro-climatological frameworks which suggest that this ratio is sufficient (under some assumptions) to determine land-surface water flux partitioning into evaporation and drainage/runoff (Budyko, 1963; Oldekop, 1911; Roderick & Farquhar, 2011; Turc, 1954). Changes in both E_o and mean precipitation may offset each other, potentially with no change in \bar{E}/E_o . Projected changes in storm characteristics, such as intensification of precipitation extremes (Kharin et al., 2013; O’Gorman & Schneider, 2009), are neglected in these frameworks.

Land surface moisture fluxes are state dependent, however (Akbar et al., 2018; Haghighi et al., 2018; Koster et al., 2018; Short Gianotti et al., 2019). Thus, changes in flux partitioning are better understood through (1) changes in the probability distribution of soil moisture (θ , the surface moisture state variable, highly inconsistent across models; Koster et al., 2009) and (2) its

downstream impacts on evaporation (E), surface runoff (R), and drainage/percolation (D). E determines surface temperatures and humidity through the surface energy balance. D and R together determine streamflow and groundwater recharge, and will be assessed together in this study as D (see discussion below). Both outfluxes, E and D , depend nonlinearly on θ . It is thus necessary to query observations of the land surface to see which changes in atmospheric forcings are expected to add linearly and which may be offsetting.

Observations of surface soil moisture (Entekhabi et al., 2010; O'Neill et al., 2016) and inferred surface moisture fluxes (Akbar et al., 2019) provide an opportunity to constrain these downstream variables. The use of historical observations to develop hydrologic response functions does not replace ESMs which couple the synchronous dynamics of atmospheric circulation, surface hydrology, and land-atmosphere feedbacks (Berg et al., 2016; Milly & Dunne, 2016; Swann, 2018). These observations instead provide a framework to assess the response of each component of the surface water balance to different climate perturbations free from model-imposed parameterizations. Additionally, daily time series allow finer temporal assessment of θ variations and the mechanisms of E/D partitioning, an advantage over use of historical annual means in other frameworks (Berghuijs et al., 2017; Greve et al., 2018; Roderick et al., 2014; Roderick & Farquhar, 2011).

This motivates our research question: How will precipitation be partitioned into evaporation and subsurface drainage fluxes in a warmer climate with changes in potential evaporation (E_o), mean precipitation (\bar{P}), and precipitation extremes?

To address this question, we use an observation-driven framework to assess how key fluxes pull the landscape water balance in opposing directions in response to climate perturbations. We use hydrologic response functions estimated from historical precipitation and satellite soil moisture observations to (a) determine evaporative and drainage responses to precipitation forcing and soil moisture state. We then (b) use the retrieved E and D response functions to determine changes in

Author Manuscript

warm-season fluxes across the Contiguous United States (ConUS) subject to perturbed (i) E_o , (ii) \bar{P} , (iii) precipitation extremes, and (iv) coincident changes in all three.

As we will find, these perturbations lend themselves well to superposition and magnitude-scaling, and so the choice of perturbation magnitudes is not particularly significant, except in relation to the magnitude of impact on E or D.

We will compare the results to typical aridity-index (Budyko) methods for estimating changes in E and D and find that changes to the precipitation distribution/extremes are critical in E/D partitioning. Finally we calculate elasticities of E and D to changes in E_o , \bar{P} , and precipitation extremes.

Methods

Water balance model and parameter estimation

To derive time series of surface soil moisture, evaporation, and drainage we follow the method of Akbar et al., (2019). Surface soil moisture for the summers (May-September) of 2015-2017 is modeled using an estimation approach with two objective functions to minimize squared differences between modeled surface microwave brightness temperatures and observations from the SMAP satellite (Entekhabi et al., 2010; O'Neill et al., 2016) while additionally conserving water mass. The problem is solved with an adjoint variational method where the water balance equation is incorporated using a Lagrange multiplier. The water balance is driven by gridded gauge-based precipitation observations from NCEP's Climate Prediction Center (Chen et al., 2008) and determines effluxes of water from the homogeneous surface layer as

$$\Delta z \cdot \frac{d\theta}{dt} = P(t) - E(\theta) - D(\theta) \quad \#(1)$$

where Δz is the thickness of the surface layer, θ is the volumetric soil moisture (modeled as uniform within the layer), $P(t)$ is the precipitation rate, $E(\theta)$ is evapotranspiration to the atmosphere, and $D(\theta)$ is drainage losses to subsurface soil layers. Four parameters — E_o , b , c , and d determine the shapes of the evaporation (E) and drainage (D) components:

$$E(\theta; E_o, b) = \frac{1}{2} \cdot \left(1 + \tanh \left[8 \left(\frac{\theta}{\phi} - \frac{1}{1 + e^{-b}} + 0.25 \right) \right] \right) \cdot E_o \quad \#(2)$$

$$D(\theta; c, d) = c \cdot \left(\frac{\theta}{\phi} \right)^d \quad \#(3)$$

for porosity ϕ . The parameters Δz , E_o , b , c , and d are estimated in Akbar et al. (2019) for each 36km SMAP pixel and create a forward water model for surface soil moisture given precipitation inputs and the previous soil moisture state. The loss functions (2) and (3) are intentionally flexible enough to span most plausible moisture/flux relations: b shifts the evaporation function as a function of soil moisture, c and d are effective Clapp-Hornberger parameters (Clapp & Hornberger, 1978). The estimated Δz determines the thickness of the surface layer that maintains hydrologic mass balance. Example evaporative and drainage loss functions are shown for a location in Southern Iowa in Figure 1a.

Climate Perturbations

To begin we impose warm-season (MJJAS) climate perturbations as 3%, 6%, 9%, and 12% increases of E_o , 2.5%, 5%, 7.5%, and 10% increases in \bar{P} , and 2.5%, 5%, 7.5%, and 10% increases in “heavy” (upper decile) precipitation, denoted P_{X90} . The values are selected as typical

of the modeled global mean (including oceans) response to 1-4°C increases in global temperature (Fläschner et al., 2016; Hartmann et al., 2013; Kharin et al., 2013; Lambert & Webb, 2008; McVicar et al., 2012; Pall et al., 2007; Pendergrass et al., 2017; Samset et al., 2016; Scheff & Frierson, 2014), but this selection is somewhat arbitrary. We assert that these perturbations are not intended to represent real forecasts of future climate. Forecasts of perturbations at local scale will depend on uncertain changes in atmospheric water vapor dynamics (Anderson et al., 2015; Byrne & O’Gorman, 2015; Dai et al., 2018; Muller et al., 2011; Prein & Pendergrass, 2019; Romps, 2011; Short Gianotti et al., 2014; Sohn & Park, 2010; Thackeray et al., 2018; Vecchi et al., 2006) and land-atmosphere-biosphere feedbacks (Greve et al., 2018; Greve & Seneviratne, 2015; Novick et al., 2016; Rigden et al., 2018), and must be estimated in fully-coupled settings (Berg et al., 2016; Berg & Sheffield, 2018; Milly & Dunne, 2016; Swann, 2018). Results from this study can then be applied to variable fields of perturbations.

To investigate water demand-only effects, the E_o parameter is perturbed at each location. E values from Equation 2 represent the soil moisture-conditioned mean-state evaporation, and hence E_o represents the mean-state potential evaporation. E itself varies at the timestep of our model (sub-daily), as it is driven by daily precipitation influxes and soil moisture states. See Figure 1b for loss function impacts.

In all scenarios, precipitation occurrence is unchanged, as is the timing of the ranked precipitation intensity (if the July 12th rain event is the 10th heaviest observed amount at a given location, this timing/ranking will remain true in all scenarios). The intensities themselves are altered by either: (a) increasing mean precipitation or (b) through an amplification of extreme events. To increase mean precipitation, intensities on all wet days are multiplied by a scaling factor $1 + m \cdot v$, using $v = 0.025$, $m = \{1,2,3,4\}$ (Figure 1c). Amplification of extreme precipitation re-allocates some precipitation from the dry tail of the intensity distribution to the wet tail in a manner which leaves both the mean and maximum precipitation unchanged (Figure

1d and Supplementary Figure 1). See Supplementary Information for further details. Note that this re-allocation has no impact on E/D partitioning in the Budyko framework.

Water Balance

The time series of θ , E , and D are determined by integrating the water balance (1) using the CPC precipitation observations at 3-minute time steps and the parameters estimated in Akbar et al. (2019) (additionally, see Akbar et al., (2019) for validation of θ against SMAP Level 3 soil moisture retrievals, D against gauged streamflow, and E against flux tower latent heat flux measurements). Explicit Hortonian overland runoff is generated when precipitation influx exceeds the storage capacity of the entire pixel, but is rare at 36km scale using 3-minute time steps. Drainage from the surface layer drives both groundwater recharge and surface streamflow in this framework; the two are not estimated separately. Seasonal mean Hortonian runoff out of the saturated pixel is $< 0.01\%$ of seasonal mean precipitation for all locations. Adding this runoff to estimated drainage fluxes has no impact on the results.

We integrate the water balance (1) using the observations (Figure 1a), the altered potential evaporation parameter (E_o experiment — Figure 1b), the altered precipitation through scaling (\bar{P} experiment — Figure 1c), and the altered precipitation through amplification of extremes (P_{X90} experiment — Figure 1d) independently to determine perturbative effects on evaporation and drainage partitioning. Examples of each experiment are shown as soil moisture time series for a single summer in Figure 1a-d. We also integrate the water balance with all interacting effects (Combined experiment) for analysis. In each case, the dynamics by which the probability distribution of soil moisture plays out through the moisture-dependent flux functions determine the aggregate flux partitioning into E and D .

Results

As found previously (Akbar et al., 2019), warm season continental evaporation under present conditions is generally larger than drainage by a factor of 2 or more (Figure 2a). As shown in Figure 1b, increasing E_o shifts the PDF of soil moisture towards drier states, decreasing the D component faster than the E component. E increases (and D decreases) by roughly 0.05-0.1 mm/day for a 3% increase in E_o in the wettest regions (Figure 2b), with notable changes in the Eastern ConUS, and minimal changes in the already water-limited West.

Increasing water supply through increased precipitation (\bar{P} experiment; Figure 2c) leads to increases in both E and D as expected, with larger magnitude increases in D in wetter, more energy-limited regions and larger magnitude increases in E in drier, more water-limited regions (effectively defined by the typical 100th parallel arid/humid division of ConUS hydroclimate). Drainage is essentially unchanged in arid regions, where existing E_o dominates surface fluxes. The shift in the soil moisture marginal distribution does not significantly increase drainage in these arid regions since the drainage function (steep only for wetter soils) is largely insensitive to soil moisture under drier conditions (see Fig. 1a).

The redistribution of precipitation from light rainfall days to heavy days (P_{X90} experiment; Figure 2d) leads to near-universal increases in D at the expense of E. This is perhaps expected due to the sensitivity of hydraulic conductivity to soil moisture, but not *a priori* certain due to the complex interplay of precipitation regimes, climatic conditions, and soil texture controls on evaporative and drainage fluxes. The dominant impacts in the Eastern US highlight the role the wet end of the precipitation and soil moisture distributions can play in seasonal-scale water budgets, effectively offsetting E_o (atmospheric demand) changes in 2b with no change to the seasonal supply.

When integrating the water balance using the combined forcings of the E_o , \bar{P} , and P_{X90} experiments, we find near-universal increases in both mean E and D across the range of changes

to E_o and precipitation (Figure 2e). As with the subcomponents shown in 2b-d, D is primarily impacted in the Eastern ConUS, while E has more-nearly-equivalent magnitude changes across climate gradients for equivalent boundary condition perturbations. Recall that water supply changes in these experiments are driven by equivalent *relative* changes, e.g., 5% of local mean precipitation, rather than absolute changes in mm/day. Mean soil moisture decreases universally across the ConUS as well for the combined experiment (Supplementary Figure 2), which is also projected in coupled model experiments (Gu et al., 2019). The largest magnitude decreases occur in the Ohio and Mississippi River Valleys, effectively shifting the arid/humid transition zone to the East.

On average across the ConUS, a 3% increase in E_o alone (spatial average of leftmost column of Figure 2b) increases E by a little more than 3 mm over a single warm season (0.017 mm/day or 1% of the ConUS-averaged E). A 2.5% increase in mean precipitation increases E by a little more than 5 mm, and a 2.5% increase in the upper decile of precipitation (transferred from the driest days) decreases E by 2.6 mm. The combined effect is an average 5.6 mm, 1.5% of the ConUS average, and equivalent to a roughly 0.82 W/m^2 latent heat equivalent. These are all roughly an order of magnitude larger than the corresponding (same sign) changes in surface soil moisture storage.

Water balance sensitivities to climate perturbations using superposition

In Figure 2 — while each location is driven by the unique local characteristics of the retrieved moisture loss functions — all locations are subject to identical relative perturbations, which would not be the case in a broader future climate change scenario. We investigate the impact of the relative perturbation magnitudes on the combined (Figure 2e) experiment in Supplementary Figures 3-5 and find similar spatial patterns with changes in E/D partitioning magnitudes. Exploring every combination of E_o , \bar{P} , and P_{X90} perturbations is infeasible, and it prompts the

question of how significant the interactions of multiple simultaneous perturbations is on changes to E/D partitioning.

We find that adding the change in evaporation ΔE (or changes in drainage ΔD) from each of the E_o , \bar{P} , and P_{X90} perturbations modeled independently is quite similar to the ΔE from imposing the perturbations separately. Figure 3a shows the difference between the rightmost column of Figure 2e ($E_o + 12\%$, $\bar{P} + 10\%$, and $P_{X90} + 10\%$, all perturbations simultaneously) and the sum of the rightmost columns of Figure 2b-d. Errors are on the order of 1% or less, suggesting counterintuitively small impact of interactions between moisture supply and demand when averaged over the warm season.

We also find that scaling the impact of a perturbation is a close approximation of the impact of a scaled perturbation. Figure 3b shows the error in estimating ΔE in the rightmost column of Figure 2e ($E_o + 12\%$, $\bar{P} + 10\%$, and $P_{X90} + 10\%$ simultaneously) as four times ΔE in the leftmost column ($E_o + 3\%$, $\bar{P} + 2.5\%$, and $P_{X90} + 2.5\%$ simultaneously). Just as for superposition errors (combining different types of perturbations), combining multiple, say, 3% perturbations of E_o to get a 12% E_o perturbation works quite well. Errors are on the order of 2% or less in terms of ΔE , and much less in terms of the total $E + \Delta E$ estimate for the season.

We find additional support for this superposability of climate perturbations by using observed E_o , \bar{P} , and P_{X90} anomalies to estimate E anomalies at eddy covariance towers in a linear regression framework (Supplementary Figure 6). Since we do not partition streamflow explicitly from groundwater recharge and landscape storage, we do not attempt a similar validation with seasonally-averaged stream gage data.

Comparison with aridity-index approach: The Budyko framework misses important dynamics

The integration of the water balance in (1)-(3) results in time series of E across the ConUS, which can then be used to fit the spatially-varying n parameter of the standard hydroclimatological Budyko curve (Choudhury, 1999) for each pixel location:

$$\frac{E}{E_o} = \frac{P}{(P^n + E_o^n)^{\frac{1}{n}}} \#(4)$$

Without the actual evaporation (E) time series, n is typically either assumed constant (often $n = 2$ as from Turc [1954], although for a single continent-wide fit we find better fit with $n = 2.24$), or n comes somewhat circularly from land surface model output, where the internal functions driving water flux partitioning are themselves parameterized. We emphasize that using model output to fit these hydroclimatological parameters without some ingested water cycle data will necessarily return results based largely on the parameters used to drive the same land surface model. We fit n for each pixel using monthly aggregated values across the warm season using total least-squares (or “errors in variables”) regression (Figure 4a), giving a spatial map of the n parameter (Figure 4b). This n estimation technique is independent of these circularities arising from use of land surface model outputs.

Changes in evaporation (ΔE) due to perturbations of E_o and \bar{P} alone are similar for the framework in this study and the Budyko-based method (Figure 4c, $r^2 = 0.88$ for $E_o + 12\%$, $r^2 = 0.96$ for $\bar{P} + 10\%$, similar for ΔD and for smaller perturbations), but with some bias. Errors between the methods are nearly entirely explained by changes in surface moisture storage, and the Budyko method’s evaporation bias for increased \bar{P} is similarly due to neglecting the shift in mean soil moisture towards wetter, more drainage-favorable conditions.

Changes in the distribution of precipitation intensities, however, have no representation in the Budyko framework (Figure 4c, $\Delta P_{X90} + 10\%$), and can be a major player in the partitioning of E and D (bias in ΔE by a factor of 2, and $r^2 = 0.58$ for all effects combined).

Elasticity of evaporation and drainage to E_o , \bar{P} , and extreme P perturbations

To assess relative impacts with more spatial granularity, we calculate the rate of change of each hydrologic response to a given climate perturbation (Supplementary Figure 7). When normalized, these are elasticities of fluxes to perturbations (Andréassian et al., 2016; Chiew, 2006; G. Fu et al., 2007; Risbey & Entekhabi, 1996; Sankarasubramanian et al., 2001; Yang & Yang, 2011). The elasticities are calculated as regression slopes of E versus E_o (normalized by observed E/E_o) for 0-12% changes in E_o , of E vs \bar{P} (normalized by observed E/\bar{P}) for 0-10% changes in \bar{P} , and of E vs P_{X90} (normalized by observed E/P_{X90}) for 0-10% changes in P_{X90} — where P_{X90} is the amount of precipitation in the upper decile of the observed precipitation distribution. P_{X90} increasing by 5% represents the wettest days originally providing 10% of seasonal average precipitation now provide 10.5% of seasonal precipitation, and the driest days contributing 0.5% of seasonal precipitation now see no rain. Elasticities for drainage are calculated similarly.

Evaporation is more sensitive to relative changes in \bar{P} than E_o (both positive elasticities) in 74% of ConUS pixels, and drainage is more sensitive to relative changes in \bar{P} than E_o in 99% of pixels. Differences between these numbers are due to the difference in effect of surface soil drying/wetting for E and D (i.e., transient climate change effects of changes in storage). The general finding that a 1% change in moisture supply \bar{P} has a larger impact on downstream fluxes than a 1% change in moisture demand E_o is typical of elasticity studies using aridity index frameworks and modeled evaporation data (Berghuijs et al., 2017).

Drainage elasticities to change in mean potential evaporation E_o and mean precipitation \bar{P} are an order of magnitude larger than for E , and with opposing signs (Supplementary Figures 7d and 7e). The shifts in precipitation extremes P_{x90} have equivalent magnitude as shifts in \bar{P} , amplifying the impacts on drainage.

Separating the ConUS into East and West halves (Supplementary Figure 8) leads to average E increases of 0.17 mm/day per each additional 1 mm/day of E_o in the East (aggregate elasticity of 0.34) versus 0.05 mm/day in the West (aggregate elasticity of 0.28). East (West) ConUS E increases by 0.35 (0.66) mm/day per 1 mm/day of additional \bar{P} , an aggregate elasticity of 0.48 (0.72). By changing precipitation extremes, E in the East (West) decreases 0.62 (0.34) mm seasonally per 1 mm of precipitation reallocated to wet days from dry days, an aggregate elasticity of -0.30 (-0.14). Actual evaporation increases slightly with increased extremes in the most arid pixels (Supplementary Figures 7 and 11) due to a shift of the soil moisture PDF from “Stage III” evaporation to “Stage II” evaporation, but magnitudes of both fluxes are vanishingly small.

Discussion and Conclusions

This study assesses the responses of evaporation and soil drainage to changes in potential evaporation, mean precipitation, and the distribution of daily precipitation intensities using a water balance framework developing observed fields of surface soil brightness temperatures and precipitation alone. These response sensitivities have been previously calculated using models, but we argue that modeled sensitivities are inherently determined by land surface parameterizations of evapotranspiration and soil moisture pedotransfer functions. This study confronts these sensitivities with data directly—in an “offline” mode with no representation of feedbacks (e.g., canopy conductance) other than that captured in the water cycle observations—and thus serves as a partial derivative of land surface moisture fluxes to climate perturbations, holding feedbacks constant. We claim that this uncoupled (but data-driven) approach serves as a

necessary counterbalance to data-blind models (but with fully coupled dynamics), and we advocate for future assimilation and reanalysis schemes incorporating dynamical land surface and vegetation data streams.

We find that the E/D partitioning response to climate perturbations is generally additive and scalable (Figure 3, Supplementary Figure 6). This is unexpected, given the nonlinearity of the loss functions and time series responses shown in Figure 1, but may prove quite useful in both parameterized land surface schemes in global climate models and in estimating climate impacts from the output of GCMs with simplified land surface hydrology representations. As an example, locally-estimated climate sensitivities for E_o , \bar{P} , and P_{X90} to surface temperature changes from a coupled model could be multiplied by the perturbation responses in Figure 2b-d for temperature-driven future scenario estimation of water flux partitioning.

There are, however, many processes that could change this linearity, including land-cover change, changes to seasonal water storage (snowpack), and land-atmosphere feedbacks such as convective triggering and changes in vegetation-controlled surface conductance and water-use efficiency. We hypothesize that the major non-linearities occur around the transition from water-limited to energy-limited states; thus, this simple additivity is unlikely to hold for shifts large enough to transition between moisture regimes (see the Central Plains, Supplementary Figure 9).

Our method for amplifying precipitation extremes is simple, and one of many possible approaches to represent this process. Actually characterizing the local changes to the precipitation distribution as a function of global mean temperature changes is likely empirically intractable, due to the magnitude of internal variability relative to low-frequency signals (Short Gianotti et al., 2014). Similarly, we do not investigate changes in the timing of precipitation (Pal et al., 2013) or storm/interstorm durations, which might expose more of the nonlinearity of the land surface flux partitioning. The results of these investigations would only be as robust as our estimation of the climate signal itself, which remains highly uncertain at this time.

While the superposability and scaling of impacts of climate perturbations is similar to the assumptions of aridity-index based hydroclimatology frameworks (Budyko), we find differences between these frameworks and our observation-driven scheme. These differences include large biases in changes to evaporation and drainage when precipitation extremes change (Figure 4). This suggests that mean-state conditions alone (E_o , seasonal P totals) are not sufficient to characterize changes to land-surface wetting of the atmosphere and surface- and ground-water resource supplies under changing climate scenarios.

Two major consequences of using our more process-based representation over a steady-state aridity-index formulation are 1) that transient changes in water storage (not part of the Budyko scheme) are significant for global change scenarios which display trends/shifts in surface moisture regimes, and 2) that assumptions embedded in aridity-index frameworks where E/D partitioning responds identically to a 10% increase in seasonal precipitation as to a 10% decrease in E_o neglect the significant nuance of water balance dynamics. We argue that both of these effects are important, and that the dynamic system state of (2) — summarized here as the probability distribution of soil moisture — plays a role in the long-term average E and D partitioning. This is shown clearly in the P_{X90} experiment in Figures 2d, 4c, and Supplementary Figure 7c,f.

GCM studies suggest trends towards drier warm season surface soils, but perhaps wetter subsurface soils (Berg et al., 2017), which align with our global mean-state perturbation experiments (Figure 2e and Supplementary Figure 2). We argue that this is the expected consequence of an increase in both water supply and water demand, and that these trends are likely to only be amplified by increases in precipitation extremes (heavy days and dry spells). A drier surface does not imply less evaporation in these scenarios, but may imply less drainage and increased buffering potential for precipitation inputs; this may explain the relative stability of flooding events relative to increasing precipitation extremes (Sharma et al., 2018).

The results of this study suggest that caution is necessary when viewing land surface conditions through a simple aridity lens when asking questions about global change. The downstream responses to water supply and demand will depend on the dynamics and distribution of land surface state variables (e.g., soil moisture). Changes in these state variables will more directly determine how the continental water cycle responds to global climate change.

References

- Akbar, R., Short Gianotti, D. J., McColl, K. A., Haghighi, E., Salvucci, G. D., & Entekhabi, D. (2018). Estimation of landscape soil water losses from satellite observations of soil moisture. *Journal of Hydrometeorology*, 19(5), 871–889. <https://doi.org/10.1175/JHM-D-17-0200.1>
- Akbar, R., Short Gianotti, D. J., Salvucci, G. D., & Entekhabi, D. (2019). Mapped Hydroclimatology of Evapotranspiration and Drainage Runoff Using SMAP Brightness Temperature Observations and Precipitation Information. *Water Resources Research*, 55, 3391–3413.
- Anderson, B. T., Gianotti, D. J., & Salvucci, G. D. (2015). Detectability of historical trends in station-based precipitation characteristics over the continental united states. *Journal of Geophysical Research*, 120(10), 4842–4859. <https://doi.org/10.1002/2014JD022960>
- Andréassian, V., Coron, L., Lerat, J., & Le Moine, N. (2016). Climate elasticity of streamflow revisited - An elasticity index based on long-term hydrometeorological records. *Hydrology and Earth System Sciences*, 20(11), 4503–4524. <https://doi.org/10.5194/hess-20-4503-2016>
- Berg, A., & Sheffield, J. (2018). Climate Change and Drought: the Soil Moisture Perspective. *Current Climate Change Reports*, 4(2), 180–191. <https://doi.org/10.1007/s40641-018-0095-0>

- Berg, A., Findell, K., Lintner, B., Giannini, A., Seneviratne, S. I., van den Hurk, B., et al. (2016). Land–atmosphere feedbacks amplify aridity increase over land under global warming. *Nature Climate Change*, 6(May). <https://doi.org/10.1038/nclimate3029>
- Berg, A., Sheffield, J., & Milly, P. C. D. (2017). Divergent surface and total soil moisture projections under global warming. *Geophysical Research Letters*, 44, 236–244. <https://doi.org/10.1002/2016GL071921>
- Berghuijs, W. R., Larsen, J. R., van Emmerik, T. H. M., & Woods, R. A. (2017). A Global Assessment of Runoff Sensitivity to Changes in Precipitation, Potential Evaporation, and Other Factors. *Water Resources Research*, 53(10), 8475–8486. <https://doi.org/10.1002/2017WR021593>
- Budyko, M. I. (1963). *Evaporation under natural conditions*. Isreal Program for Scientific Translations.
- Byrne, M. P., & O’Gorman, P. A. (2015). The response of precipitation minus evapotranspiration to climate warming: Why the “Wet-get-wetter, dry-get-drier” scaling does not hold over land. *Journal of Climate*, 28(20), 8078–8092. <https://doi.org/10.1175/JCLI-D-15-0369.1>
- Chen, M., Shi, W., Xie, P., Silva, V. B. S., Kousky, V. E., Higgins, R. W., & Janowiak, J. E. (2008). Assessing objective techniques for gauge-based analyses of global daily precipitation. *Journal of Geophysical Research Atmospheres*, 113(4), 1–13. <https://doi.org/10.1029/2007JD009132>
- Chiew, F. H. S. (2006). Estimation of rainfall elasticity of streamflow in Australia. *Hydrological Sciences Journal*, 51(4), 613–625. <https://doi.org/10.1623/hysj.51.4.613>
- Choudhury, B. J. (1999). Evaluation of an empirical equation for annual evaporation using field

observations and results from a biophysical model. *Journal of Hydrology*, 216(1–2), 99–110. [https://doi.org/10.1016/S0022-1694\(98\)00293-5](https://doi.org/10.1016/S0022-1694(98)00293-5)

Clapp, R. B., & Hornberger, G. M. (1978). Empirical Equations for Some Soil Hydraulic Properties. *Water Resources Research*, 14(4), 601–604.

Dai, A., Zhao, T., & Chen, J. (2018). Climate Change and Drought: a Precipitation and Evaporation Perspective. *Current Climate Change Reports*, 4(3), 301–312. <https://doi.org/10.1007/s40641-018-0101-6>

Entekhabi, D., Njoku, E. G., O'Neill, P. E., Kellogg, K. H., Crow, W. T., Edelstein, W. N., et al. (2010). The Soil Moisture Active Passive (SMAP) Mission. *Proceedings of the IEEE*, 98(5), 704–716. <https://doi.org/10.1109/JPROC.2010.2043918>

Fläschner, D., Mauritsen, T., & Stevens, B. (2016). Understanding the intermodel spread in global-mean hydrological sensitivity. *Journal of Climate*, 29(2), 801–817. <https://doi.org/10.1175/JCLI-D-15-0351.1>

Fu, G., Charles, S. P., & Chiew, F. H. S. (2007). A two-parameter climate elasticity of streamflow index to assess climate change effects on annual streamflow. *Water Resources Research*, 43(11), W11419. <https://doi.org/10.1029/2007WR005890>

Fu, Q., & Feng, S. (2014). Responses of terrestrial aridity to global warming. *Journal of Geophysical Research: Atmospheres*, 119, 7863–7875. <https://doi.org/10.1002/2014JD021608>

Greve, P., & Seneviratne, S. I. (2015). Assessment of future changes in water availability and aridity. *Geophysical Research Letters*, 42(13), 5493–5499. <https://doi.org/10.1002/2015GL064127>

Greve, P., Orlowsky, B., Mueller, B., Sheffield, J., Reichstein, M., & Seneviratne, S. I. (2014).

Global assessment of trends in wetting and drying over land. *Nature Geoscience*, 7(10), 716–721. <https://doi.org/10.1038/NGEO2247>

Greve, P., Gudmundsson, L., & Seneviratne, S. I. (2018). Regional scaling of annual mean precipitation and water availability with global temperature change. *Earth System Dynamics*, 9(1), 227–240. <https://doi.org/10.5194/esd-9-227-2018>

Gu, X., Zhang, Q., Li, J., Singh, V. P., Liu, J., Sun, P., & Cheng, C. (2019). Attribution of Global Soil Moisture Drying to Human Activities: A Quantitative Viewpoint. *Geophysical Research Letters*, 1–10. <https://doi.org/10.1029/2018GL080768>

Haghighi, E., Short Gianotti, D. J., Akbar, R., Salvucci, G. D., & Entekhabi, D. (2018). Soil and Atmospheric Controls on the Land Surface Energy Balance: A Generalized Framework for Distinguishing Moisture- and Energy-Limited Evaporation Regimes. *Water Resources Research*, 1–21. <https://doi.org/10.1002/2017WR021729>

Hartmann, D. L., Tank, A. M. G. K., Rusticucci, L. V., Alexander, S. B., Charabi, Y., Dentener, F. J., et al. (2013). *Observations: Atmosphere and Surface. Climate Change 2013 the Physical Science Basis: Working Group I Contribution to the Fifth Assessment Report of the Intergovernmental Panel on Climate Change* (Vol. 9781107057). Cambridge, UK and New York, NY, USA: Cambridge University Press. <https://doi.org/10.1017/CBO9781107415324.008>

Hawkins, E., & Sutton, R. (2011). The potential to narrow uncertainty in projections of regional precipitation change. *Climate Dynamics*, 37(1), 407–418. <https://doi.org/10.1007/s00382-010-0810-6>

Hirabayashi, Y., Mahendran, R., Koirala, S., Konoshima, L., Yamazaki, D., Watanabe, S., et al. (2013). Global flood risk under climate change. *Nature Climate Change*, 3(9), 816–821. <https://doi.org/10.1038/nclimate1911>

- Kharin, V. V., Zwiers, F. W., Zhang, X., & Wehner, M. (2013). Changes in temperature and precipitation extremes in the CMIP5 ensemble. *Climatic Change*, 119(2), 345–357. <https://doi.org/10.1007/s10584-013-0705-8>
- Koster, R. D., Guo, Z., Yang, R., Dirmeyer, P. A., Mitchell, K., & Puma, M. J. (2009). On the nature of soil moisture in land surface models. *Journal of Climate*, 22(16), 4322–4335. <https://doi.org/10.1175/2009JCLI2832.1>
- Koster, R. D., Crow, W. T., Reichle, R. H., & Mahanama, S. P. (2018). Estimating Basin-Scale Water Budgets With SMAP Soil Moisture Data. *Water Resources Research*, 54(7), 4228–4244. <https://doi.org/10.1029/2018WR022669>
- Lambert, F. H., & Webb, M. J. (2008). Dependency of global mean precipitation on surface temperature. *Geophysical Research Letters*, 35(16), 1–5. <https://doi.org/10.1029/2008GL034838>
- McVicar, T. R., Roderick, M. L., Donohue, R. J., Li, L. T., Van Niel, T. G., Thomas, A., et al. (2012). Global review and synthesis of trends in observed terrestrial near-surface wind speeds: Implications for evaporation. *Journal of Hydrology*, 416, 182–205. <https://doi.org/10.1016/j.jhydrol.2011.10.024>
- Milly, P. C. D., & Dunne, K. A. (2016). Potential evapotranspiration and continental drying. *Nature Climate Change*, 6, 946–951. <https://doi.org/10.1038/NCLIMATE3046>
- Muller, C. J., O’Gorman, P. A., & Back, L. E. (2011). Intensification of precipitation extremes with warming in a cloud-resolving model. *Journal of Climate*, 24(11), 2784–2800. <https://doi.org/10.1175/2011JCLI3876.1>
- Novick, K. A., Ficklin, D. L., Stoy, P. C., Williams, C. A., Bohrer, G., Oishi, A. C., et al. (2016). The increasing importance of atmospheric demand for ecosystem water and carbon fluxes.

Nature Climate Change, 1(September), 1–5. <https://doi.org/10.1038/nclimate3114>

- O’Gorman, P. A., & Schneider, T. (2008). The hydrological cycle over a wide range of climates simulated with an idealized GCM. *Journal of Climate*, 21(15), 3815–3832. <https://doi.org/10.1175/2007JCLI2065.1>
- O’Gorman, P. A., & Schneider, T. (2009). The physical basis for increases in precipitation extremes in simulations of 21st-century climate change. *Proceedings of the National Academy of Sciences of the United States of America*, 106(35), 14773–14777. <https://doi.org/10.1073/pnas.0907610106>
- O’Gorman, P. A., Allan, R. P., Byrne, M. P., & Previdi, M. (2012). Energetic Constraints on Precipitation Under Climate Change. *Surveys in Geophysics*, 33(3–4), 585–608. <https://doi.org/10.1007/s10712-011-9159-6>
- O’Neill, P. E., Chan, S., Njoku, E. G., Jackson, T., & Bindlish, R. (2016). SMAP L3 Radiometer Global Daily 36 km EASE-Grid Soil Moisture, Version 4. Boulder, Colorado USA: NASA National Snow and Ice Data Center Distributed Active Archive Center. <https://doi.org/10.5067/OBBHQ5W22HME>
- Oldekop, E. (1911). *Evaporation from the surface of river basins (Испарение съ поверхности речныхъ бассейновъ)*. University of Tartu-Jurjew-Dorpat, Tartu, Estonia.
- Pal, I., Anderson, B. T., Salvucci, G. D., & Gianotti, D. J. (2013). Shifting seasonality and increasing frequency of precipitation in wet and dry seasons across the U.S. *Geophysical Research Letters*, 40(15), 4030–4035. <https://doi.org/10.1002/grl.50760>
- Pall, P., Allen, M. R., & Stone, D. A. (2007). Testing the Clausius-Clapeyron constraint on changes in extreme precipitation under CO2 warming. *Climate Dynamics*, 28(4), 351–363. <https://doi.org/10.1007/s00382-006-0180-2>

- Pendergrass, A. G., Knutti, R., Lehner, F., Deser, C., & Sanderson, B. M. (2017). Precipitation variability increases in a warmer climate. *Scientific Reports*, 7(1), 1–9. <https://doi.org/10.1038/s41598-017-17966-y>
- Prein, A. F., & Pendergrass, A. G. (2019). Can we Constrain Uncertainty in Hydrologic Cycle Projections? *Geophysical Research Letters*, (2018), 2018GL081529. <https://doi.org/10.1029/2018GL081529>
- Rigden, A. J., Salvucci, G. D., Entekhabi, D., & Short Gianotti, D. J. (2018). Partitioning Evapotranspiration Over the Continental United States Using Weather Station Data. *Geophysical Research Letters*, 45(18), 9605–9613. <https://doi.org/10.1029/2018GL079121>
- Risbey, J. S., & Entekhabi, D. (1996). Observed Sacramento Basin streamflow response to precipitation and temperature changes and its relevance to climate impact studies. *Journal of Hydrology*, 184(3–4), 209–223. [https://doi.org/10.1016/0022-1694\(95\)02984-2](https://doi.org/10.1016/0022-1694(95)02984-2)
- Roderick, M. L., & Farquhar, G. D. (2011). A simple framework for relating variations in runoff to variations in climatic conditions and catchment properties. *Water Resources Research*, 47(6), 1–11. <https://doi.org/10.1029/2010WR009826>
- Roderick, M. L., Sun, F., Lim, W. H., & Farquhar, G. D. (2014). A general framework for understanding the response of the water cycle to global warming over land and ocean. *Hydrology and Earth System Sciences*, 18(5), 1575–1589. <https://doi.org/10.5194/hess-18-1575-2014>
- Romps, D. M. (2011). Response of Tropical Precipitation to Global Warming. *Journal of the Atmospheric Sciences*, 68(1), 123–138. <https://doi.org/10.1175/2010jas3542.1>
- Samset, B. H., Myhre, G., Forster, P. M., Hodnebrog, Andrews, T., Faluvegi, G., et al. (2016). Fast and slow precipitation responses to individual climate forcings: A PDRMIP multimodel

study. *Geophysical Research Letters*, 43(6), 2782–2791.
<https://doi.org/10.1002/2016GL068064>

Sankarasubramanian, A., Vogel, R. M., & Limbrunner, J. F. (2001). Climate elasticity of streamflow in the United States. *Water Resources Research*, 37(6), 1771–1781.
<https://doi.org/10.1029/2000WR900330>

Scheff, J., & Frierson, D. M. W. (2014). Scaling potential evapotranspiration with greenhouse warming. *Journal of Climate*, 27(4), 1539–1558. <https://doi.org/10.1175/JCLI-D-13-00233.1>

Schewe, J., Heinke, J., Gerten, D., Haddeland, I., Arnell, N. W., Clark, D. B., et al. (2014). Multimodel assessment of water scarcity under climate change. *Proceedings of the National Academy of Sciences*, 111(9), 3245–3250. <https://doi.org/10.1073/pnas.1222460110>

Sharma, A., Wasko, C., & Lettenmaier, D. P. (2018). If Precipitation Extremes Are Increasing, Why Aren't Floods? *Water Resources Research*, 54(11), 8545–8551.
<https://doi.org/10.1029/2018WR023749>

Short Gianotti, D. J., Anderson, B. T., & Salvucci, G. D. (2014). The potential predictability of precipitation occurrence, intensity, and seasonal totals over the continental United States. *Journal of Climate*, 27(18), 6904–6918. <https://doi.org/10.1175/JCLI-D-13-00695.1>

Short Gianotti, D. J., Rigden, A. J., Salvucci, G. D., & Entekhabi, D. (2019). Satellite and Station Observations Demonstrate Water Availability's Effect on Continental-Scale Evaporative and Photosynthetic Land Surface Dynamics. *Water Resources Research*, 55(1), 540–554.
<https://doi.org/10.1029/2018WR023726>

Sohn, B. J., & Park, S. C. (2010). Strengthened tropical circulations in past three decades inferred from water vapor transport. *Journal of Geophysical Research Atmospheres*,

115(15), 1–9. <https://doi.org/10.1029/2009JD013713>

Swann, A. L. S. (2018). Plants and Drought in a Changing Climate. *Current Climate Change Reports*, 4(2), 192–201. <https://doi.org/10.1007/s40641-018-0097-y>

Thackeray, C. W., DeAngelis, A. M., Hall, A., Swain, D. L., & Qu, X. (2018). On the Connection Between Global Hydrologic Sensitivity and Regional Wet Extremes. *Geophysical Research Letters*, 45(20), 11,343–11,351. <https://doi.org/10.1029/2018GL079698>

Turc, L. (1954). The water balance of soils: relationship between precipitations, evaporation and flow (Le bilan d'eau des sols: relation entre les précipitations, l'évaporation et l'écoulement). *Annales Agronomiques, Série A*, 5, 491–595.

Vecchi, G. A., Soden, B. J., Wittenberg, A. T., Held, I. M., Leetmaa, A., & Harrison, M. J. (2006). Weakening of tropical Pacific atmospheric circulation due to anthropogenic forcing. *Nature*, 441(1), 73–76. <https://doi.org/10.1038/nature04744>

Yang, H., & Yang, D. (2011). Derivation of climate elasticity of runoff to assess the effects of climate change on annual runoff. *Water Resources Research*, 47(7), 1–12. <https://doi.org/10.1029/2010WR009287>

Acknowledgements

Soil moisture (SMAP) data are available from the National Snow and Ice Data Center portal (<http://www.nsidc.org>). Precipitation data are available from the NCEP ftp portal (ftp.cpc.ncep.noaa.gov/precip/CPC_UNI_PRCP/). The authors acknowledge no conflicts of interest.

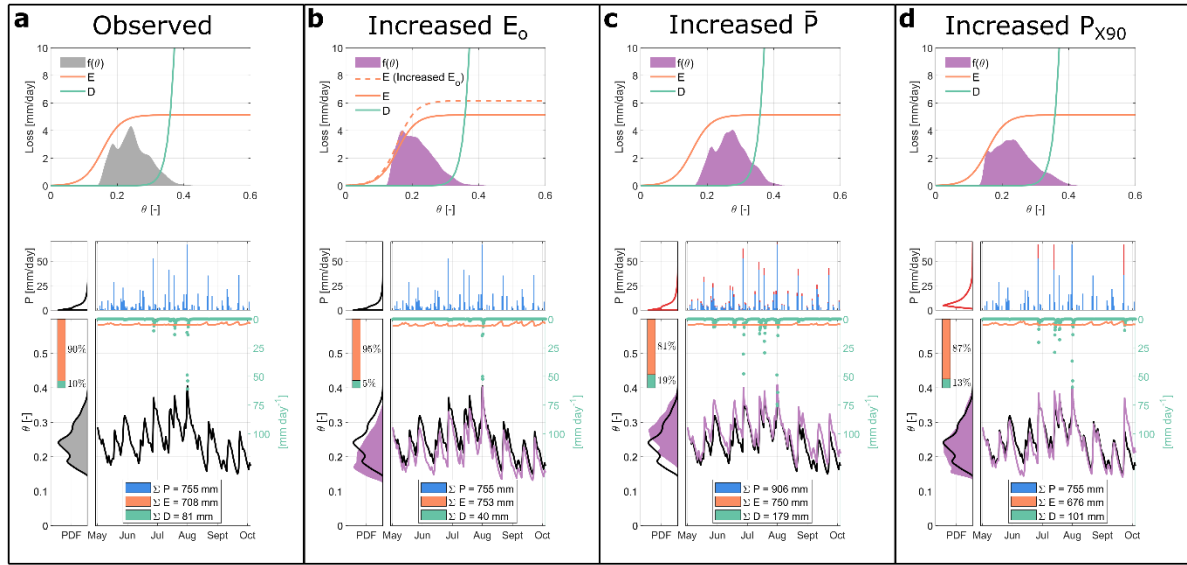


Figure 1: Example evaporation and drainage loss losses for observations and experimental perturbations for a location in Southern Iowa, summer 2015. a) Retrieved evaporation (E) and drainage (D) loss functions; observed precipitation (P); and time series of soil moisture (θ), E, and D based on observations. Grey shaded regions show the marginal probability density (PDF) of soil moisture $f(\theta)$. Blue bars show daily precipitation with accompanying PDF for wet days. Black line, orange line, and green markers show θ , E, and D time series (E and D shown on right axis). Orange (green) bar shows E's (D's) fractional contribution to seasonal outfluxes from the land surface. b) Same as (a), except for the increased potential evaporation (E_o) experiment using the orange dashed line for $E(\theta)$. Precipitation unchanged, but $f(\theta)$ moves towards drier conditions where E losses dominate D. c) Same as (a) except for with increased daily precipitation, shown as red bars above observed (blue) precipitation bars. $f(\theta)$ (in red) shifts to wetter conditions, increasing D. d) Same as (a) except with increased precipitation extremes (mean and maximum daily P unchanged). Red P bars show added precipitation on wet

days, taken from an equal amount of precipitation removed on drier days. $f(\theta)$ (in red) increases the wet tail at the expense of the dry tail, leading to increased D_0 and reduced E .

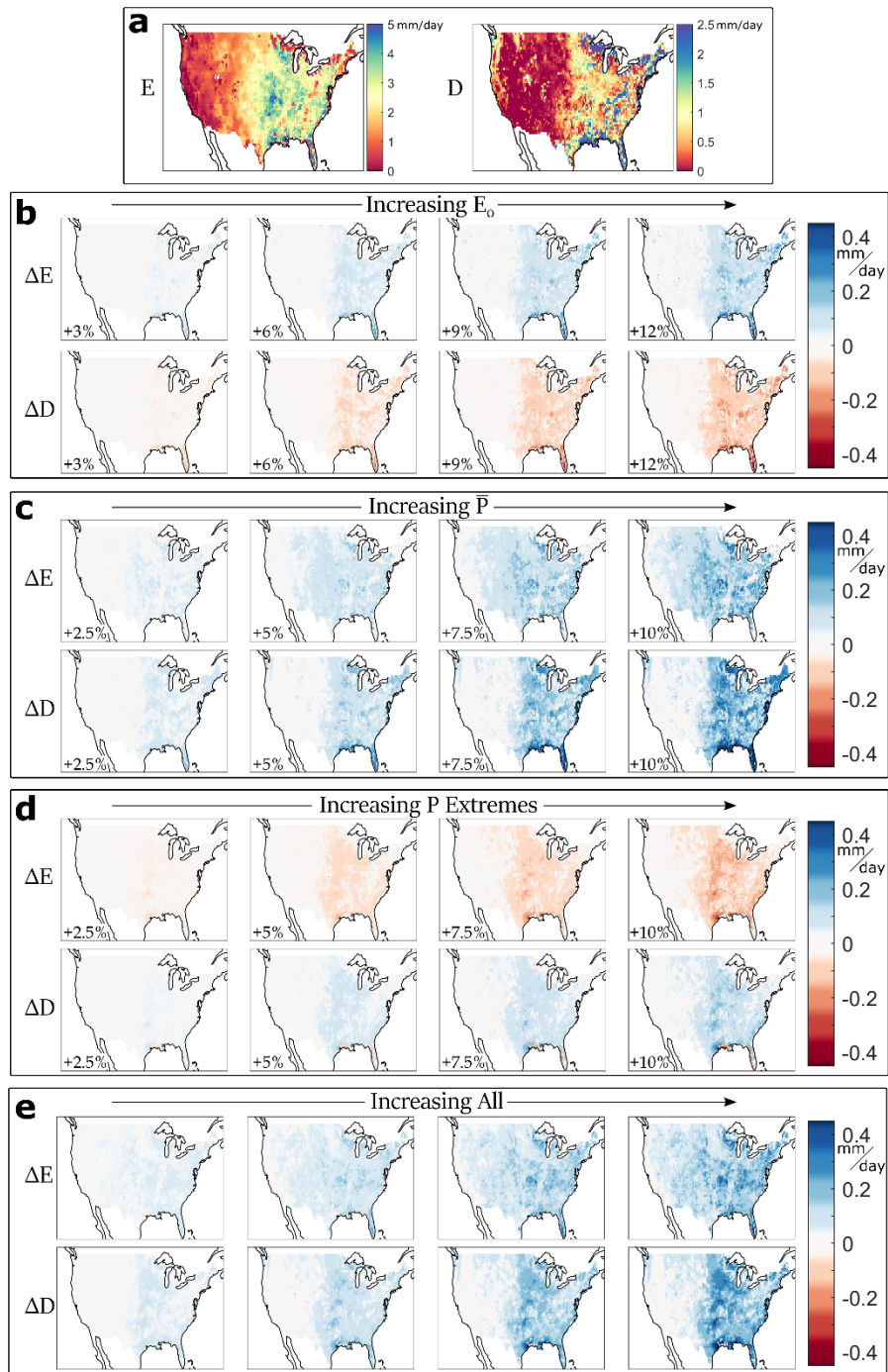


Figure 2: Evaporation, drainage, and hydrologic sensitivities to climate perturbations. a) Mean evaporation (E) and drainage (D) for warm season 2015–2017 from the estimated loss functions and climate perturbations. b) First column shows changes ΔE and ΔD relative to (a) for a 3% increase in E_o . Columns 2–4 show impacts for E_o increases of 6%, 9%, and 12%. Evaporation increases across the ConUS and drainage decreases, with the most substantial changes in the energy-limited East. c) Same as (b) but for perturbations to \bar{P} . d) Same as (b) but for increases in extreme precipitation (percentages show heaviest decile increase — no change in \bar{P}). e) Changes in mean E and D when simultaneously combining the impacts of increased E_o , \bar{P} , and precipitation extremes.

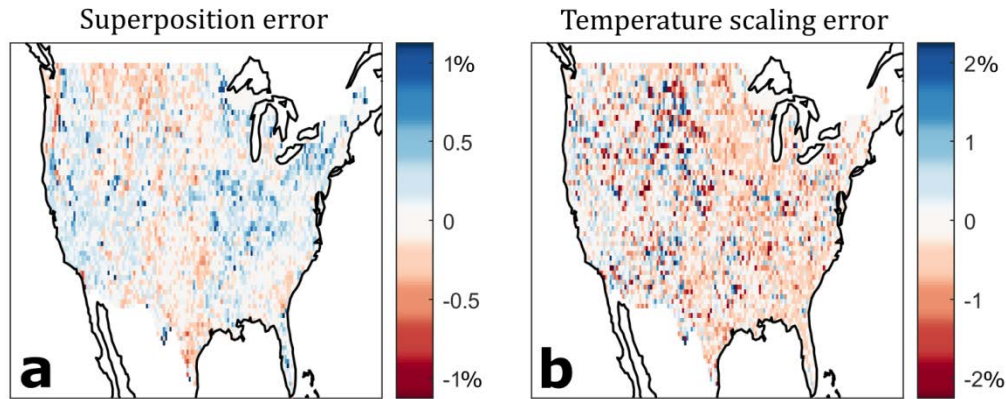


Figure 3: Superposability and scaling of individual perturbations. a) The percentage error in evaporation when adding the individual E_o , mean P, and extreme P perturbations (the sum of the rightmost column of Figure 2b-d) in place of the fully-coupled system (rightmost column of Figure 2e). b) The percentage error in evaporation when assuming linear temperature-equivalent scaling of perturbations (4 times the leftmost column of Figure 2e in place of the rightmost column of Figure 2e). Both the superposition errors and the scaling errors are small (~ 1 -2%), suggesting that the effects shown in Figure 2b-d can be combined and scaled directly based on local estimated climate sensitivities of E_o , \bar{P} , and P extremes. See also Supplementary Figures 9-10.

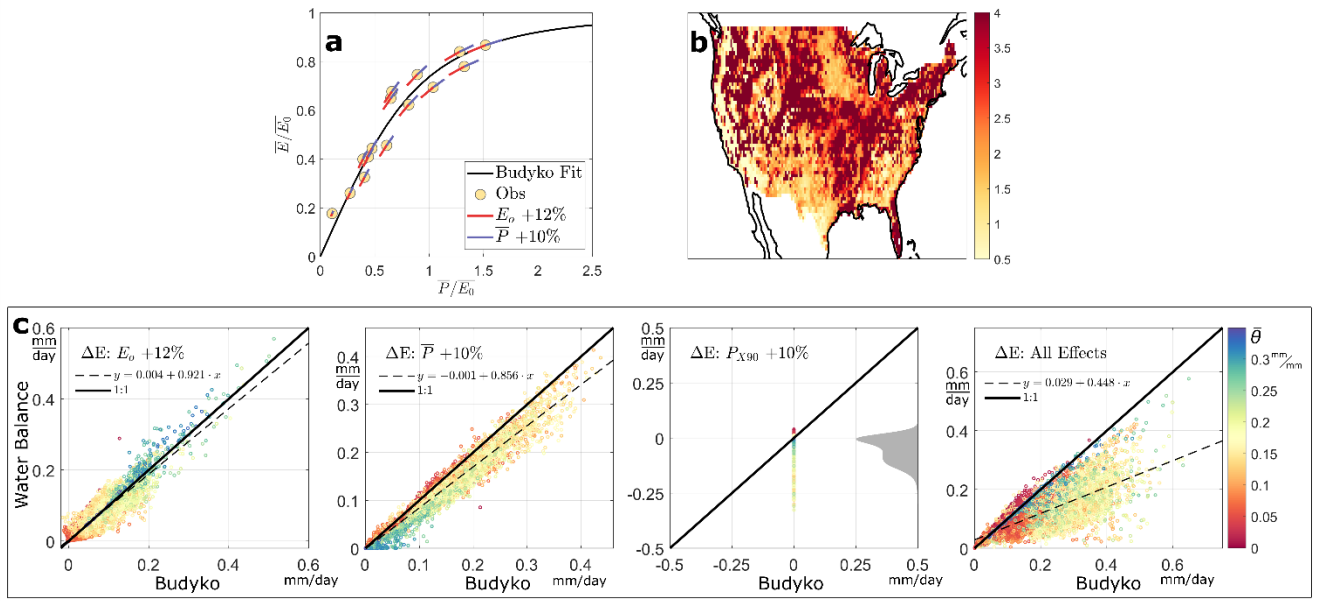
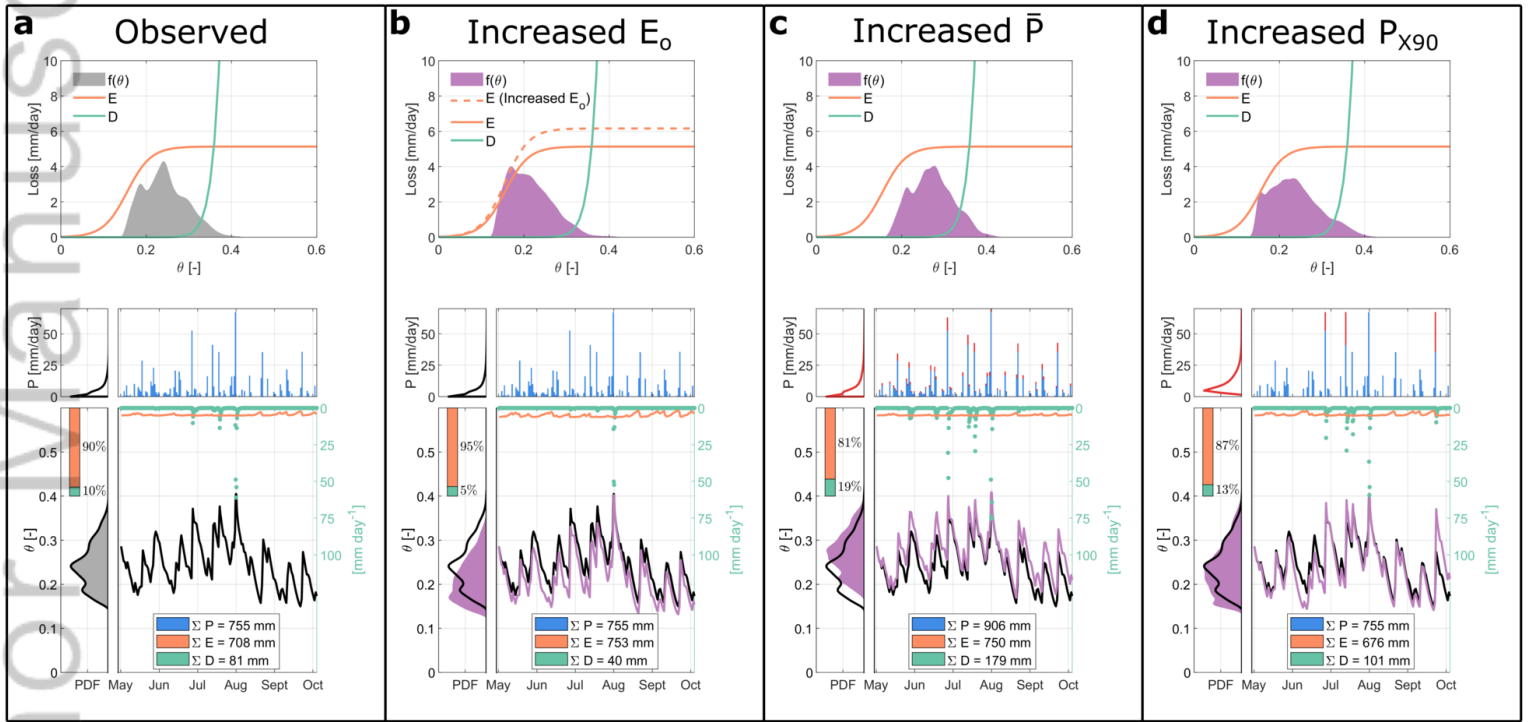
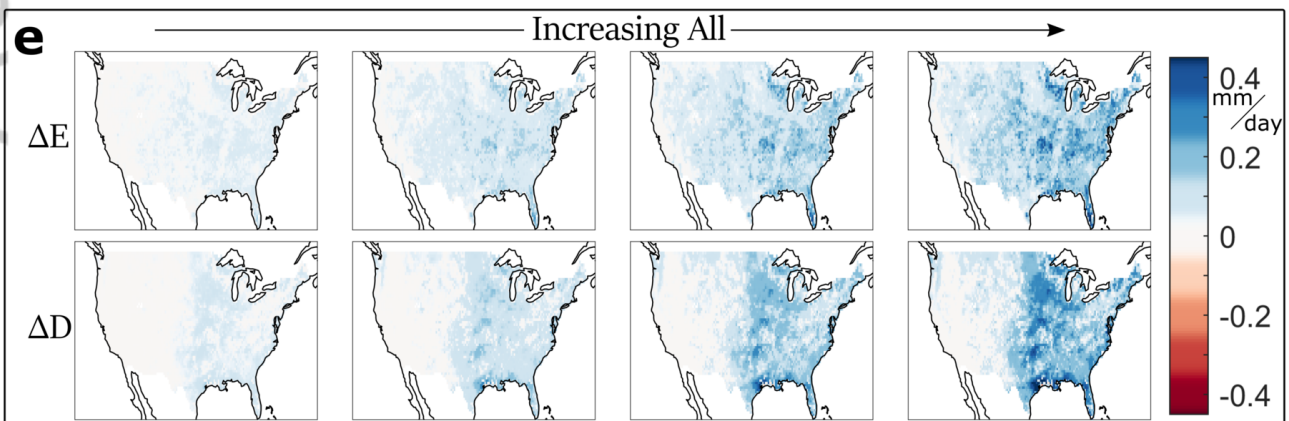
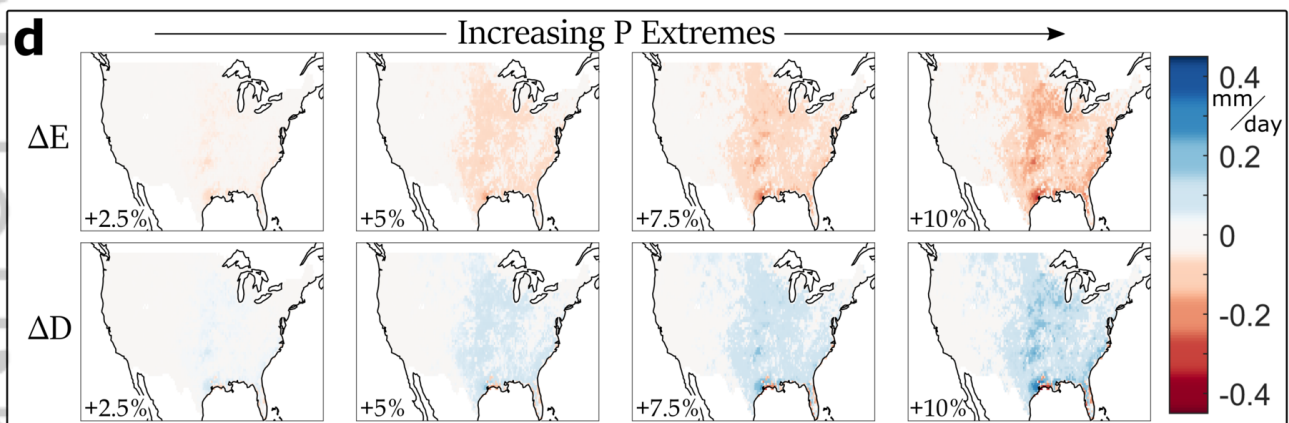
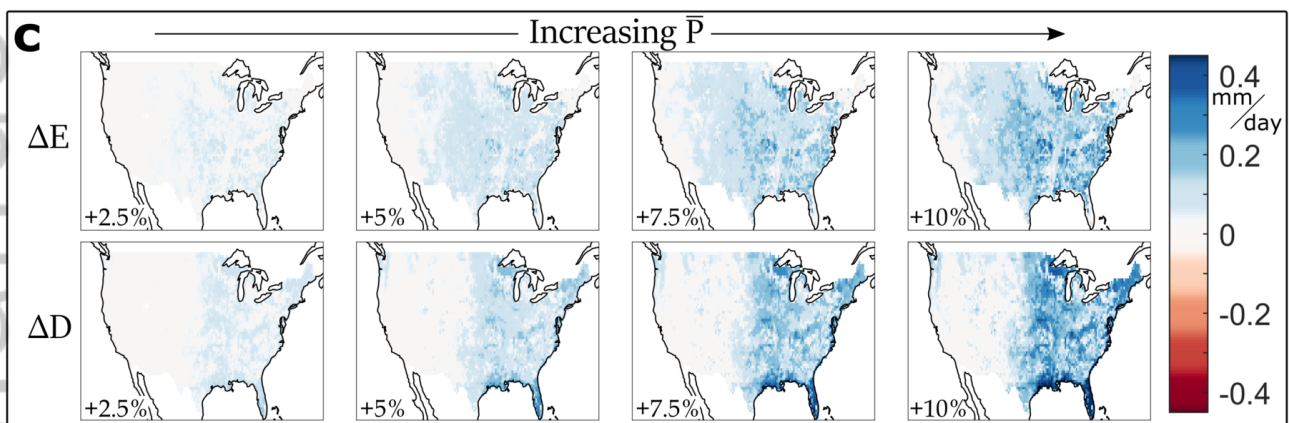
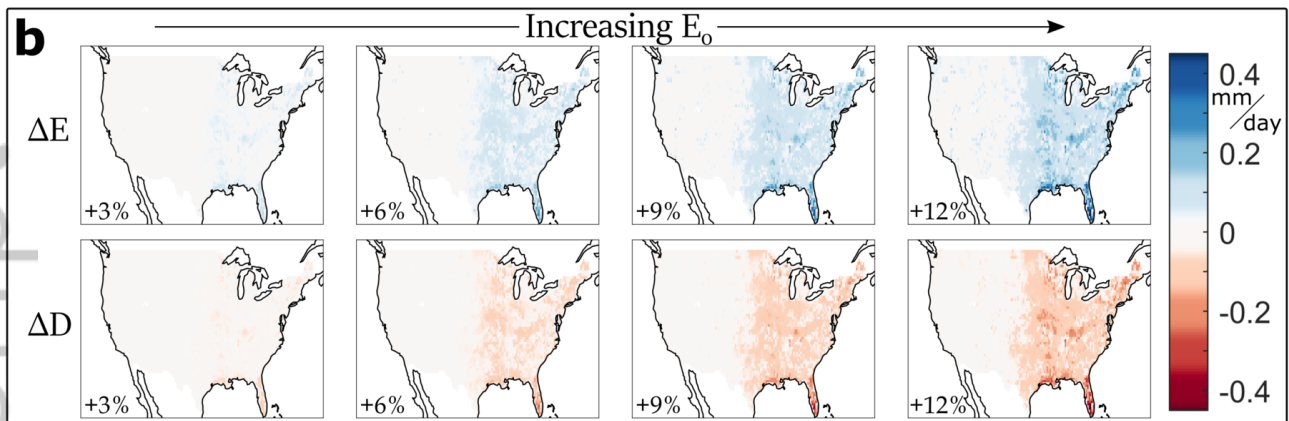
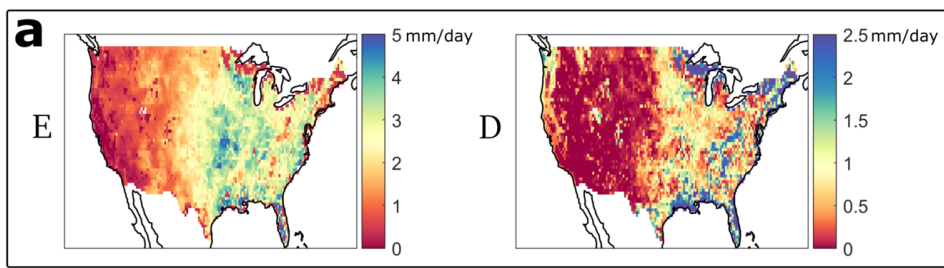


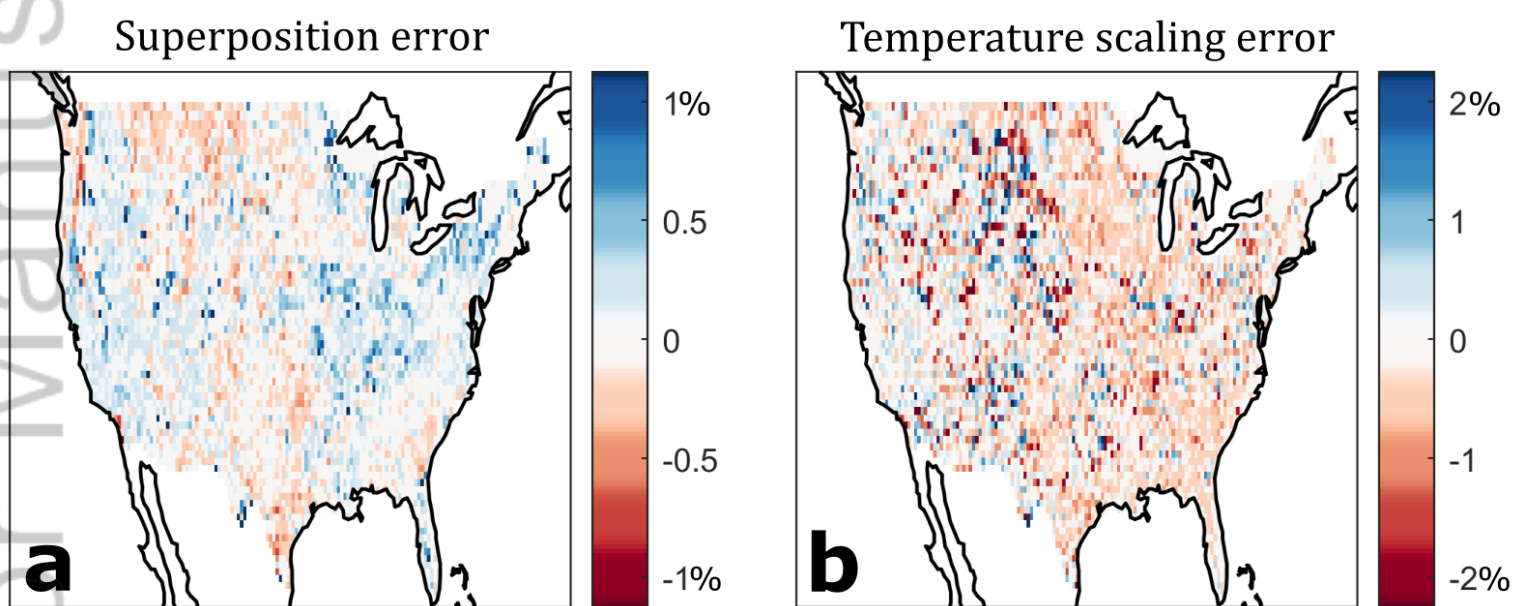
Figure 4: Comparison with Budyko hydroclimatological framework. a) The classical Budyko curve fit to a single location. Each point is a month of mean evaporation \bar{E} versus mean precipitation \bar{P} , both normalized by potential evaporation E_o . Evaporation time series and estimated potential evaporation are from the integration of the water balance (1)-(3). Lines show the shift in \bar{E}/E_o that follows a change in \bar{P}/E_o by changing E_o (red) or \bar{P} (blue). Equal E_o and \bar{P} changes cancel each other. b) The estimated Budyko n parameter for each location: $\bar{E} = \bar{P} \cdot E_o \cdot (\bar{P}^n + E_o^n)^{-\frac{1}{n}}$. c) Comparison of changes in evaporation ΔE versus the Budyko method. Plots show comparison for increased E_o , increased \bar{P} , increased precipitation extremes (P_{X90}), and all simultaneous effects combined. Colors show mean soil moisture calculated as part of the water balance. Bias in increased \bar{P} comparison due primarily to changes in soil water storage. Bias in All Effects comparison due primarily to impact of precipitation extremes.



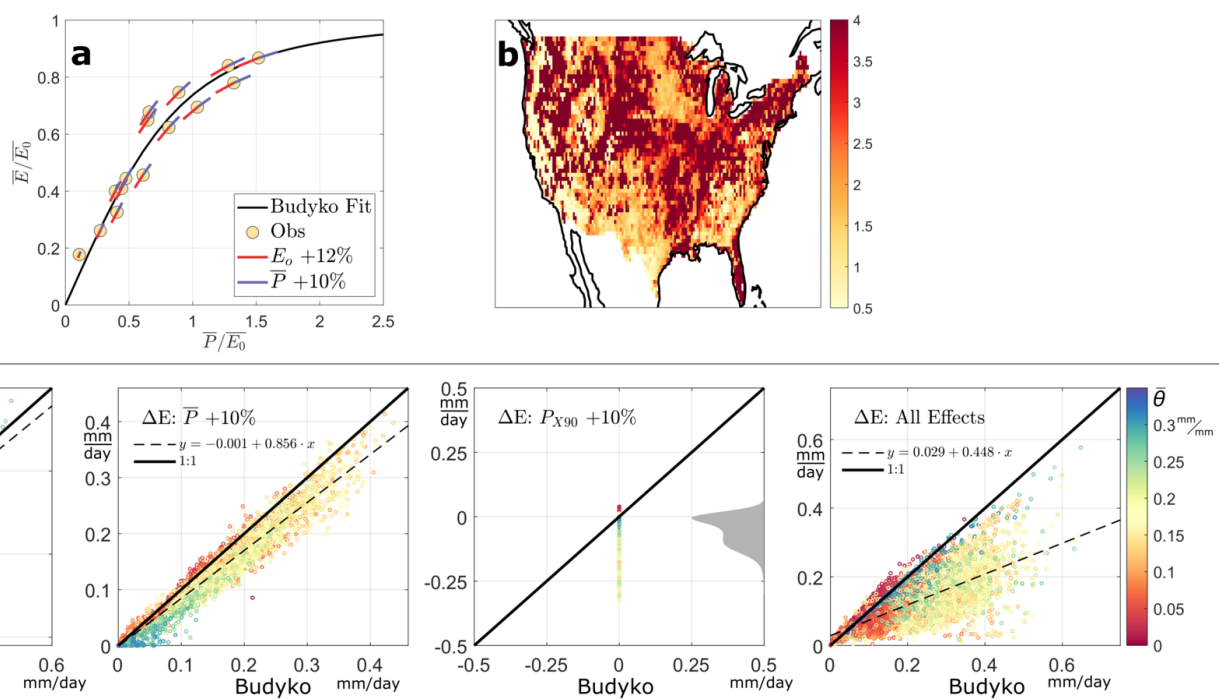
2019GL086498-f01-z.png



2019GL086498-f02-z.png



2019GL086498-f03-z-.png



2019GL086498-f04-z.png